The 3D groundwater salinity distribution and fresh groundwater volumes in the Mekong Delta, Vietnam, inferred from geostatistical analyses.

5   Jan L. Gunnink [1], Hung Van Pham[2,3], Gualbert H.P Oude Essink[3,4] and Marc F.P. Bierkens[3,4].

[1] TNO Geological Survey of the Netherlands

[2] Division of Water Resources Planning and Investigation for the South of Vietnam (DWRPIS), Ho Chi Minh city, Vietnam

[3] Department of Physical Geography, Utrecht University, the Netherlands

10   [4] Department of Subsurface and Groundwater Systems, Deltares, the Netherlands

Correspondence to Jan Gunnink: jan.gunnink@tno.nl

Abstract

Over the last decades, economic developments in the Vietnamese Mekong delta have led to a sharp increase in groundwater pumping for domestic, agricultural and industrial use. This has resulted in
15   alarming rates of land subsidence and groundwater salinization. Effective groundwater management, including strategies to work towards sustainable groundwater use, requires knowledge about the current groundwater salinity distribution, in particular the available volumes of fresh groundwater. At the moment, no comprehensive dataset of the spatial distribution of fresh groundwater is available. To create a 3D model of Total Dissolved Solids (TDS), an existing geological model of the spatial
20   distribution and thickness of the aquifers and aquitards is updated. Next, based on the sedimentological description of the borehole data, maps of drainable porosity for each aquifer are interpolated. Measured TDS in groundwater, inferred TDS from resistivity measurements in boreholes and soft incomplete data from domestic wells are combined in an indicator kriging routine to obtain the full probability distribution of TDS for each (x,y,z) location. This statistical distribution of TDS
25   combined with drainable porosity yields estimates of the volume of fresh groundwater (TDS < 1 g/L) in each aquifer. Uncertainty estimates of these volumes follow from a Monte Carlo analysis (sequential indicator simulation). Results yield an estimated fresh groundwater volume for the Mekong delta of 867 billion m^3 with an uncertainty range of 830-900 billion m^3, which is somewhat higher than previous assessments of fresh groundwater volumes. The resulting dataset can be used
30   to support informed groundwater management decisions, e.g. to prevent further salinization of aquifers and land subsidence and are available at https://doi.org/10.5281/zenodo.4441776 (Gunnink et al, 2021)

1. Introduction

A large part of the world's population lives in deltas, many of which are located in developing
35   countries. In these areas, there is a great demand for fresh water for domestic, agricultural and industrial use (Wada et al., 2011; Gioassan et al., 2014; Tessler et al., 2015; Syvitski et al., 2009; Van Engelen et al, 2019. This places large strains on the available freshwater resources, being mostly surface water and groundwater. In Vietnam, there is a rapidly growing awareness that the interrelated issues of depletion of water resources and salt water intrusion will probably negatively affect the
40   economic development potential of the country, including the Mekong delta (Renaud and Kuenzer,

2012; Nguyen et al., 2001; Tam et al., 2014; Tran et al., 2012; Larsen et al., 2017). Since Vietnam's economic reform policy was introduced in 1986, urbanization and intensification of agriculture and aquaculture led to a drastic increase in groundwater exploitation in the Mekong delta (Minderhoud et al., 2017; Wagner et al., 2012). At present, the total quantity of groundwater extracted from the delta is assessed to be more than 900 million m^3/year from over half a million wells in shallow and deep aquifers (Bui et al., 2013; Minderhoud et al., 2017). In addition, it is estimated that about 50% of the population in the delta depends on fresh groundwater for domestic, agricultural and industrial purposes (Bui et al., 2013; Shrestha et al., 2016). Bui et al (2013) estimated that approximately 600 billion m^3 fresh groundwater is available in the aquifers of the Mekong delta. Notwithstanding this apparent large volume, over-exploitation of fresh groundwater resources occurs, causing lateral salt water intrusion into the groundwater system, upconing of brackish to saline groundwater under extraction wells and land subsidence (Bui et al., 2013; Erban et al., 2014; Minderhoud et al., 2017; Rahman et al., 2019). Recharge of groundwater is thought to be limited due to low gradients and the predominantly clay sediments that top the groundwater system (Pham et al., 2019). Current over-exploitation of fresh groundwater reserves is evident from declining hydraulic heads throughout the delta (Wagner et al., 2012; Minderhoud et al., 2017) and from detailed studies in specific parts, e.g. the Tra Vinh province (Van and Koontanakulvong, 2019) and the Ca Mau province (Jenn et al., 2017). Furthermore, climate change scenarios indicate that groundwater levels and recharge in the Mekong delta will decline, both in the short and long term (Shrestha et al., 2016). Careful management of groundwater resources is also important to counteract the effects overexploitation has on Arsenic in groundwater. Groundwater extraction is causing interbedded clays to compact and expel water containing dissolved arsenic or arsenic-mobilizing solutes (Erban et al, 2013). This might impose additional risk to groundwater quality in the long term.

The Mekong delta is the third largest delta in the world (Coleman and Roberts 1989). It is located in the southern part of Vietnam and measures 39.700 km^2 (Pham et al., 2019). The Mekong and the Saigon delta system share the same depositional basin, such that their deposits and groundwater systems are interconnected. Therefore, the study area, as depicted in Fig. 1, is referred to as the Mekong delta (MKD) from now on. The MKD is flat, except for a few hills and has an extremely low mean elevation of about 0.8 m above mean sea level (MSL) (Minderhoud et al., 2019).
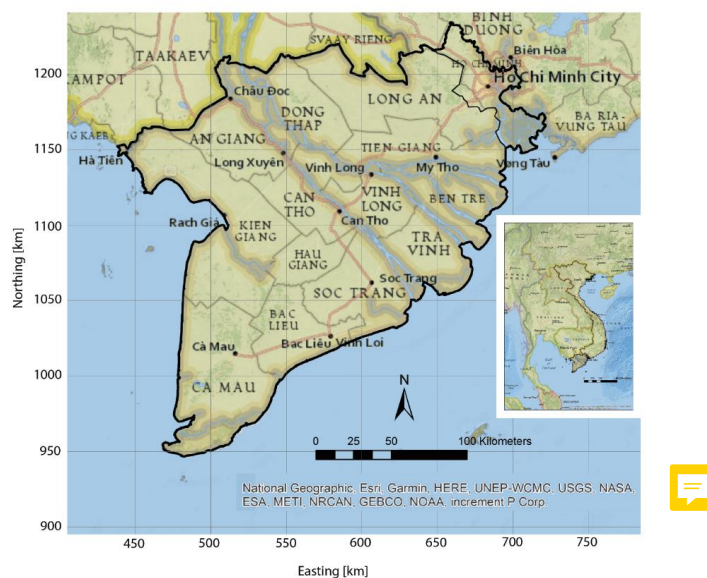
70

Figure 1 *The study area (referred to as the Mekong Delta (MKD) in this paper) includes the Mekong Delta itself as well as a part of the Saigon river delta in the Northeast around Ho Chi Minh City; coordinate system WGS84-UTM 48 N. Smaller map indicates the Mekong Delta (shaded area) as part of Vietnam.*

The objective of this research is to use state-of-the-art geostatistical methods to create a dataset of
75 the 3D groundwater salinity distribution in the aquifers of the MKD (~~viz. in gram Total Dissolved Solids
per litre, g/L TDS~~ as a measure of groundwater salinity) to provide water managers and policy makers
with an accurate assessment of the spatially varying fresh groundwater volumes, including its
uncertainty. This up-to-date dataset of the available fresh groundwater volumes, open accessible to
the community is required to effectively manage fresh groundwater resources and to develop
80 groundwater extraction strategies while minimizing negative effects, all leading to a sustainable
groundwater use (Hamer et al, 2019). Furthermore, 3D numeric models, that predict groundwater
salinization due to e.g. increased groundwater extractions and accelerated sea-level rise, need
information regarding the current 3D distribution of groundwater salinity.

To our knowledge, this is the first time that the fresh groundwater volume on a large, delta scale is
85 estimated by means of the geostatistical interpolation technique indicator kriging, which provides for
each location (x,y,z) the entire probability distribution of TDS. Indicator kriging offers the advantage
of incorporating "soft" data from additional sources and is preferred to the more often used Ordinary
Kriging method when the underlying statistical distribution is departing strongly from a Gaussian (or
at least symmetric) model. Also unique is the determination of uncertainty of the fresh groundwater
90 volumes of the individual aquifers of the MKD and the MKD as a whole. New is also that soft data from
industrial extraction wells and especially an abundant dataset of domestic wells is used on top of
numerous boreholes with geophysical loggings and groundwater samples. Also, including the spatial
variation of effective porosity to calculate fresh groundwater volumes is novel. The geostatistical
framework used to map the 3D groundwater salinity as shown here can be also applied to other delta's
95 where similar fresh groundwater volumes are under stress, such as the Nile delta (Van Engelen, et al.,
2019), the Red River delta (Larsen et al., 2017) and the Ganges-Brahmaputra-Meghnadelta (Faneca
Sànchez et al., 2015).

2. Data and methods

2.1 General approach

100 To assess the 3D groundwater salinity distribution and the associated fresh groundwater volumes including uncertainty, measurements of Total Dissolved Solids (TDS) in boreholes were combined with boreholes with geophysical loggings - including resistivity - and data of industrial and domestic extractions wells. Spatial modelling of TDS was done using geostatistical interpolation and simulation techniques. Geostatistics is widely used to assimilate data from different sources for estimating

105 variables at unvisited locations, using the spatial correlation that is inherent in many spatial datasets. Fig. 2 provides the complete workflow used to arrive at a 3D groundwater salinity distribution (in g/L TDS) and fresh groundwater volumes, where the red numbers in the right upper corner of each step denote the sections and subsections where each step is described hereafter and the arrows the relationships and information flows between the steps. The workflow consists of the following steps:

110 i) assembling a dataset of TDS measurements of varying quality from TDS measurements in boreholes, resistivity profiles in borelogs (2.4.1 and 2.4.2) and industrial and domestic extraction wells (2.4.3); ii) creating a dataset of depth-averaged drainable porosity values (2.4.4); iii) constructing an updated hydrogeological layer model (aquifers and aquitards discretized into voxels) from the existing model of Minderhoud et al. (2017), lithological descriptions in borelogs and ordinary kriging (2.5 and 3.1); iv);

115 creating maps of drainable porosity from depth averaged data using ordinary kriging (Appendix C); v) estimating the 3D groundwater salinity distribution (in g/L TDS) per aquifer and aquitard using indicator kriging (3.2.4); vi) deriving the fresh groundwater volume per aquifer and per province, for the entire MKD (3.2.5 and 3.2.7); and its uncertainty bounds using sequential indicator simulation (3.2.6 and 3.2.7).

120
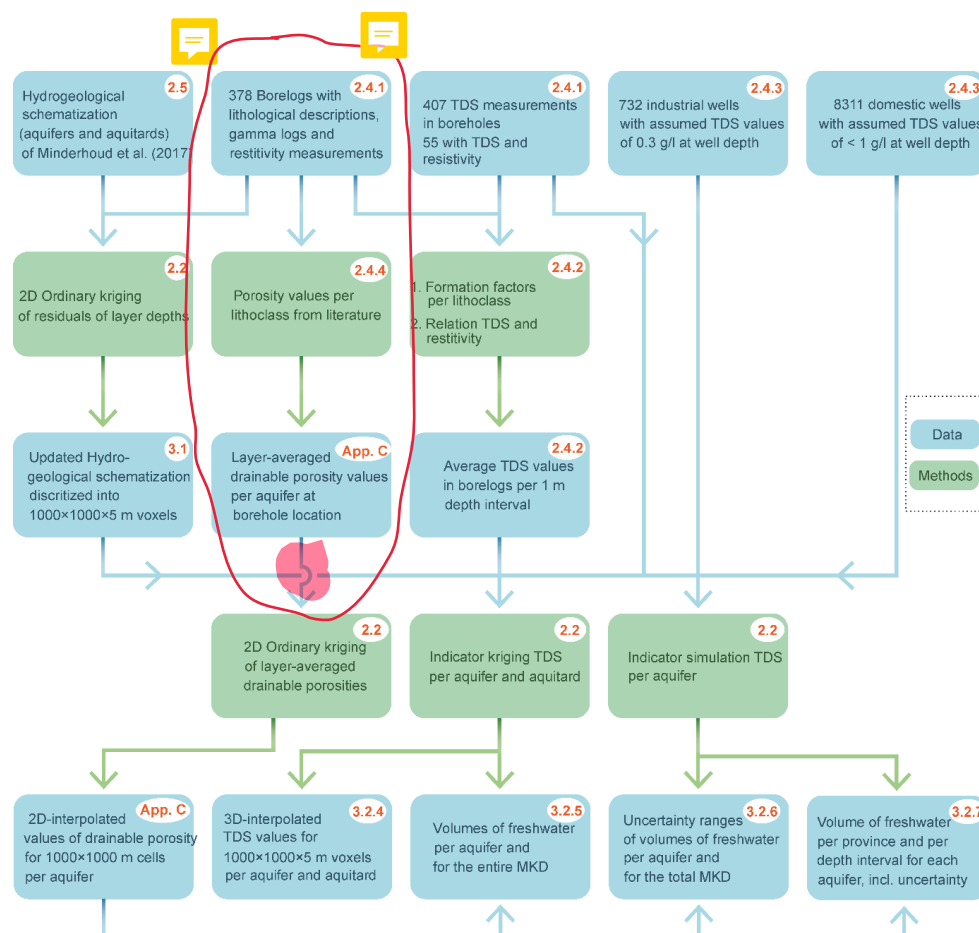
Figure 2 *Workflow of assessing the 3D groundwater salinity distribution (in g/L TDS) and the fresh groundwater volumes in the Mekong Delta, Vietnam. Red numbers provide sections and subsections where data and methods are described.*

2.2 Geostatistical modeling

There are many ways to interpolate from point observations onto a grid (Li and Heap, 2008). Among these, interpolation based on geostatistical modeling has the advantage over many deterministic methods in that a. it inherently corrects for data redundancy from clustered data, b. it explicitly uses information about the spatial structure of the variable at hand, and c. it also provides the variance of the interpolation error as a measure of uncertainty (Caers, 2011). The most basic form of geostatistical interpolation is ordinary kriging (Journel and Huijbregts, 1978), which can be generally applied for unbiased linear estimation of the unknown value at an interpolation location. Ordinary kriging, which is suitable for variables that are well described by a Gaussian distribution, was used to interpolate the base of aquifers and aquitards and the drainable porosity values. However, as shown hereafter, the groundwater salinity distributions in each aquifer are very skewed, which makes the kriging variance of ordinary kriging a poor measure of uncertainty (Goovaerts, 1997).

Moreover, to assess the fresh groundwater volume of an aquifer, at each gridcell the conditional cumulative probability of TDS, given its *n* surrounding observations of TDS is needed. To estimate this conditional probability, indicator kriging (Journel, 1983) was used. In general, one needs to estimate

140 for a variable Z(**u**) for each location **u** on the 3D grid (with **u** a vector of spatial coordinates): F(**u**; z| n)) = Prob {Z(**u**) ≤ z|(n) }. Indicator kriging estimates conditional probabilities for a finite number of thresholds and interpolates between these thresholds to estimate conditional probabilities for any value of Z. By accumulating these probabilities for each threshold, the conditional cumulative density function (ccdf) is calculated. As estimate $Z^*(\boldsymbol{u})$ of the unknown value of $Z(\boldsymbol{u})$, usually the mean

145 of the estimated conditional distribution (E-type estimate) is used (Saisna et al., 2004).

With results of indicator kriging it is possible to estimate from the conditional distribution of TDS the probability that fresh groundwater is found at a single location, and from this, an estimate of the expected fresh groundwater volume at this location. However, to estimate the expected volume of groundwater of e.g. an entire aquifer, the joint probability of finding fresh groundwater at many

150 locations in an aquifer needs to be calculated. The most straightforward way to estimate such spatial uncertainty measures is to revert to geostatistical simulation where realizations of the underlying conditional random function (conditional to the observations) are simulated and the fresh groundwater volume of each realization is estimated. By repeating this many times, many samples of the aquifer-scale fresh groundwater volume are obtained from which an empirical probability

155 distribution is obtained. In accordance with indicator kriging, sequential indicator simulation was used for this purpose.

2.3 Hydrogeology of the Mekong Delta

Here, a short description of the hydrogeology of the MKD is presented, based on Bui et al. (2013), Minderhoud et al. (2017) and Pham et al (2019). For a more comprehensive overview see Appendix A

160 The sediments in the MKD were deposited in a NW-SE oriented graben that was formed as a result of Cenozoic rifting and date from the early Miocene to the present. Seven geohydrological units are distinguished, that, in general, contain a lower part of coarse to fine sand (aquifer) and an upper part of silts and clay (aquitard). The unconsolidated sediments can be very thick, in the coastal areas more than 600 m. The seven aquifers in the study area are: Holocene (qh), Late Pleistocene (qp$_3$) , Late -

165 middle Pleistocene (qp$_{2-3}$), Early Pleistocene (qp$_1$), Middle Pliocene (n$_2^2$), Early Pliocene (n$_2^1$) and Late Miocene (n$_1^3$)

2.4 Data processing

In this section, the available data and the data transformation techniques are described that are used to arrive at a dataset that is input for spatial interpolation and simulation. The main data sources are

170 the boreholes with the description of lithology and resistivity, supplemented by both industrial and domestic abstraction wells.

2.4.1 Data collection

The database of the Division of Water Resources Planning and Investigation for the South of Vietnam (DWRPIS) was queried to obtain relevant data for the modeling of each hydrogeological unit and

175 groundwater salinity distribution (TDS): 378 borehole descriptions with geophysical loggings and lithological description of the sediments, 732 industrial abstraction wells and 407 groundwater samples that contained TDS concentrations. The data were collected during the 1980s until 2015 and were interpreted into hydrogeological units by hydrogeologists of DWRPIS. The borehole interpretation was aided by natural gamma measurements that were collected in the borehole;

180 temperature and bulk electrical resistivity were also recorded. In Fig. 3 the spatial distribution of the data is shown for each aquifer. Due to limited data for aquifer n$_1^3$, this aquifer was excluded from further analysis. The borehole data were aggregated into 1 m intervals, for reasons of efficiency and to obtain a more uniform dataset. This aggregation was done with respect to the borders of the

hydrogeological units so that no aggregation occurs over the borders of different units. The variables that were used for further analysis include lithological description, long normal (LN64) resistivity (also called bulk resistivity, representing the resistivity of the sediments ánd the groundwater), the temperature of the groundwater and classification into hydrogeological units, see Fig. 4 for some examples of typical geophysical logs.
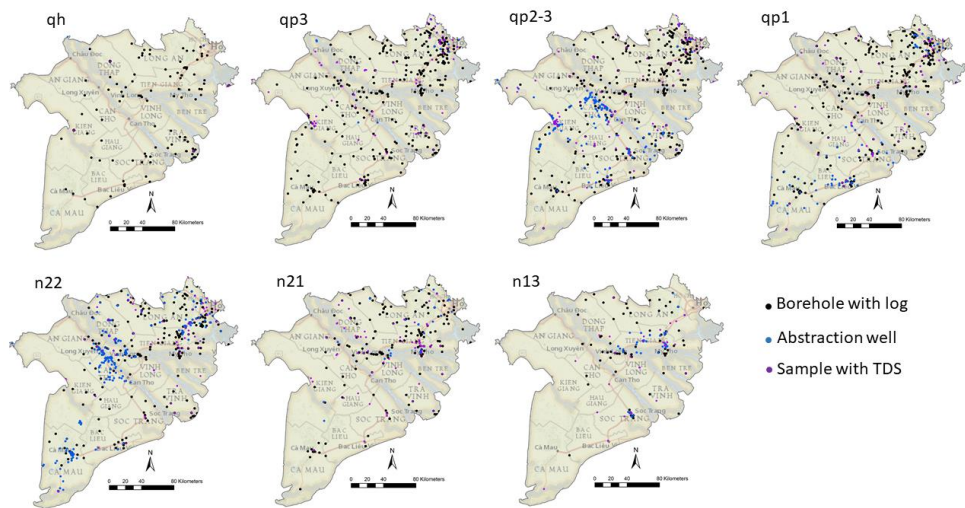
Figure 3 *Spatial distribution of the used data that is applied for each aquifer. The data density for the deepest aquifer – n_1^3 – is not sufficient to produce adequate estimates of groundwater salinity concentrations and is therefore discarded from further analysis. Copyright maps, see Fig. 1.*
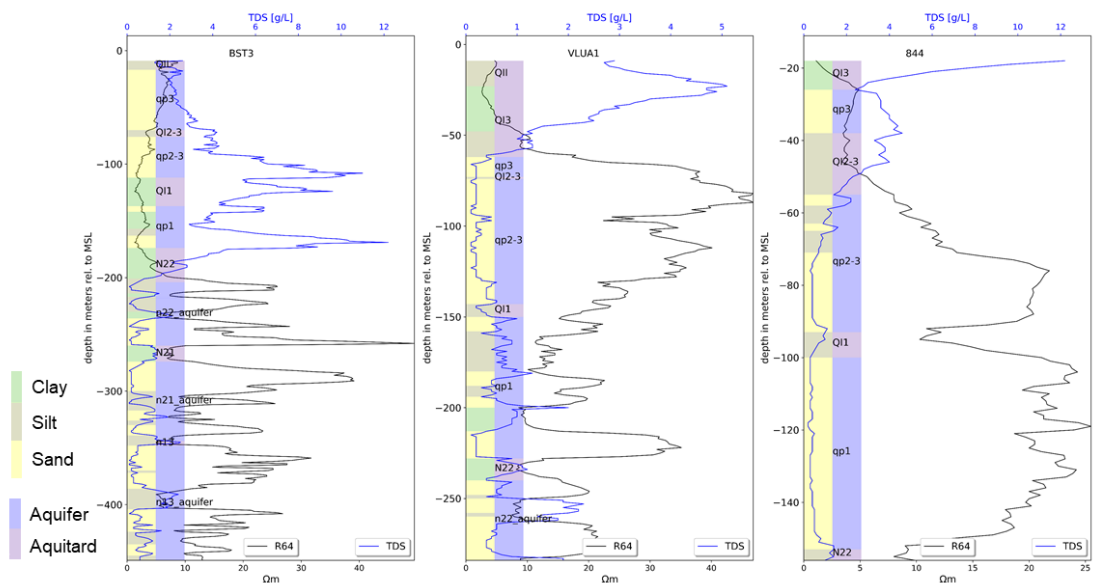
Figure 4 *Typical geophysical logs (black line) and borehole description, resulting in TDS concentrations (blue line).*

195

2.4.2 From borehole-logging to TDS

The intrinsic Formation Factor (F_i) relates the bulk resistivity of a fully saturated granular medium to the fluid resistivity. Archie (1942) defined F_i as the ratio of bulk resistivity over fluid (water) resistivity (ρ_{bulk} / ρ_w) and is valid for clay-free, consolidated sediments. However, the sediments in the Mekong

200   Delta are not clay-free and are unconsolidated, rendering the use of Archie's formula invalid, as discussed by e.g. Huntley (1986) and Worthington (1993). For clayey, unconsolidated sediments, the ratio of bulk resistivity over fluid resistivity is called the apparent Formation Factor, F_a. A modification of the Archie equation is proposed by Huntley (1986) and Worthington (1993) and applied by e.g. Soupios et al. (2007), to obtain F_a. In Appendix B the procedure to obtain F_a is described, and also the

205   validation of the resulting F_i using an independent dataset. The resulting F_i for each lithology is used to convert LN64 to ρ_w.

Table 1. Formation Factor and drainable porosity for lithology classes. The intrinsic Formation Factor (F_i) from literature (De Louw et al., 2011; Faneca-Sànchez et al., 2012) and in brackets F_i as checked by comparison with TDS-Ec(groundwater) data from Buschman et al. (2008) and An et al (2014). Drainable porosity based on Johnson

210   *(1967).*

Lithology	Intrinsic Formation Factor F_i [-]	Drainable porosity [-]
Gravel	7 (-)	0.23
coarse sand	5-6 (5.0)	0.27
medium sand	4-4.5 (4.3)	0.26
fine sand	3-3.5 (3.0)	0.21
Silt	2-2.8 (2.0)	0.08
clay / peat	1-1.5 (-)	0.02

To obtain TDS from ρ_w, a regression between the electrical conductivity (Ec, reciprocal of ρ_w) and TDS was established, based on the 55 samples with TDS and ρ_w (Fig. 5). This regression was applied to all 1 m intervals in the boreholes with LN64 measurements - in total 81250 m – resulting in 36% of the in

215   intervals in the boreholes having TDS < 1 g/L and 68% < 3 g/L.
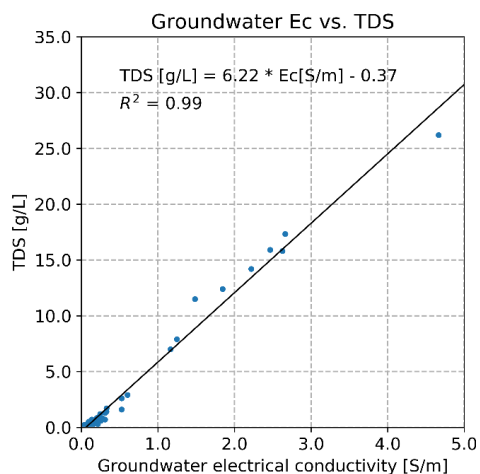
Figure 5 *Linear regression between Electrical conductivity of groundwater and TDS.*

2.4.3 Additional (soft) data sources of TDS estimates

220 Industrial extraction wells

The DWRPIS database contained data from industrial extraction wells that extract groundwater in excess of 200 m³/day. These wells often produce large volumes of drinking water for villages and towns and for industrial and agricultural purposes. The depth and the aquifer from which the groundwater is extracted is stored in the database. The TDS of the extraction wells in the database 225 was uniformly set to 0.3 g/L.

Domestic extraction wells

There are a large number of households in the MKD that have their own groundwater well for domestic use. Most of these wells are drilled by local companies and are unregulated. The location, depth and volume of groundwater extracted are not known. DWRPIS has carried out an investigation 230 to obtain basic data - location of wells and the aquifer from which the groundwater is extracted - for part of these wells in 2010, see Fig. 6 (Bui et al., 2013). No data on the quality of the water or the depth of extraction is available. To obtain the depth interval from which the water is extracted, the average depth-interval - relative to the top of the aquifer - from the boreholes that contain TDS < 1g/L in the corresponding aquifer for that area, was calculated. This average depth-interval was 235 subsequently used as a proxy for the depth interval for the domestic wells. The extracted groundwater is used for domestic purposes and was therefore assumed to have a TDS < 1 g/L. The locations of domestic extraction wells are extremely dense and clustered. The domestic extraction data was aggregated into averages of 5000 x 5000 m to prevent the abundant domestic well data to overwhelm the other data on TDS.

240
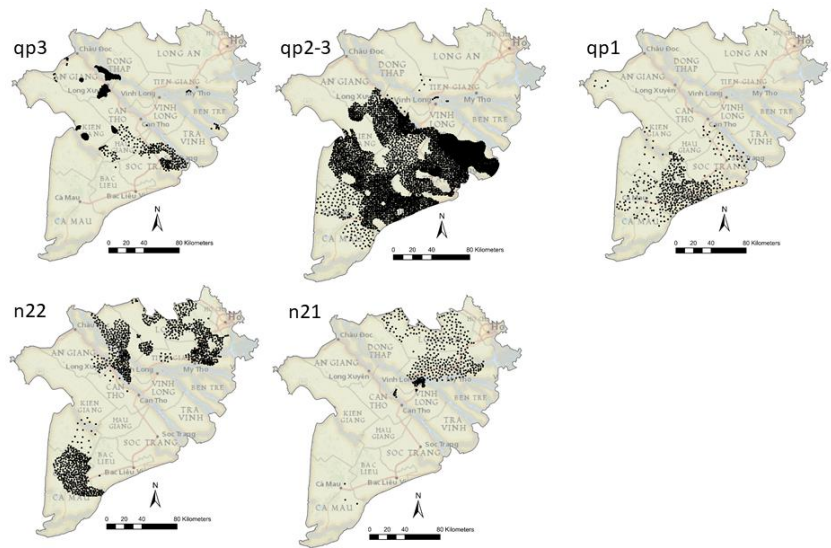
Figure 6 *Spatial distribution of domestic extraction wells in the MKD, with known location and aquifer from which the groundwater is extracted. No data for the Holocene aquifer, qh, is available, because of its predominant brackish / saline nature. Copyright maps, see Fig. 1.*

245   2.4.4 Drainable porosity

To determine the amount of potential extractable groundwater from each aquifer, the spatially distributed drainable porosity is needed. Drainable porosity indicates that part of the total volume of an aquifer that drains under gravity (Fitts, 2002) and is also called effective porosity. It is presented as a volume ratio and thus dimensionless. Data for drainable porosity of aquifers in the MKD are limited.
250   To derive at a spatial differentiated model (2D map) of drainable porosity for each aquifer, the procedure as described in Appendix C is followed. The basis data regarding drainable porosity are taken from Johnson (1967), see Table 1.

2.5 Three-dimensional modeling of aquifers and aquitards

To estimate the spatially distributed fresh groundwater volume - including uncertainty - in each
255   aquifer of the MKD, a model of the top and bottom of each hydrogeological unit in the subsurface is required. Minderhoud et al. (2017) constructed - based on 95 boreholes – a hydrogeological model (cell size 1000 x 1000 m^2) of the MKD. The larger dataset used in this study consist of the interpreted base of the hydrogeological units from boreholes and extraction wells (Fig. 3), which were used to update the basic model to a new, more detailed model. The procedure is described in detail in
260   Appendix D. The resulting layer model was converted into a voxel model (dimensions of the voxel 1000 m x 1000 m x 5 m^3) by assigning the appropriate hydrogeological unit to each voxel. The top of the voxel model was formed by the Digital Elevation Model (DEM), derived from Minderhoud et al. (2017).

3. Results

3.1 Three-dimensional model of aquifers and aquitards

265   Fig. 7 presents the updated hydrogeological model of the aquifers (lower case names) and aquitards (upper case names) in the study area up to a depth of max. 600 m. The model depicts considerable detail, showing aquifers that can have thicknesses up to 10's of meters.
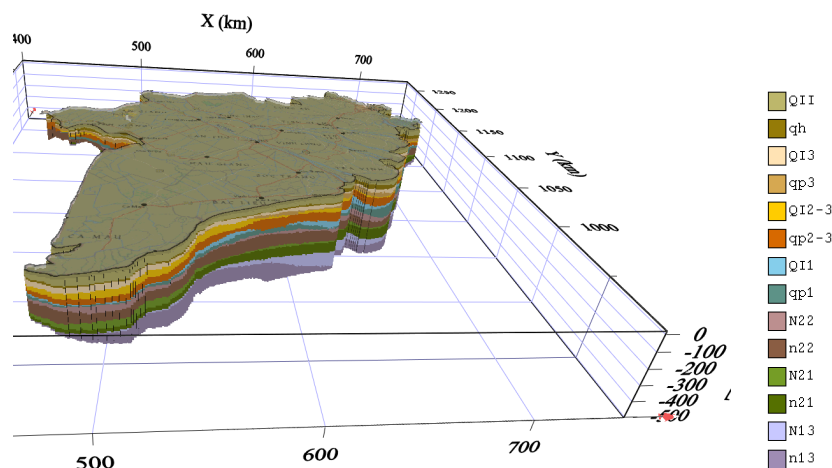
270   ***Figure 7*** *Updated hydrogeological block-model. Scale according to kilometer reading along the axis (km) and depth in meters. Vertical exaggeration 100x.*

3.2 Geostatistical analysis of TDS

3.2.1 Statistical distribution of TDS data and indicator coding

Fig. 8 shows the frequency distribution of TDS for each aquifer based on the TDS derived from the
275   boreholes with geophysical logging, groundwater samples and data from industrial extraction wells. TDS varies between the different aquifers and also between the aquifers and aquitards of the same hydrogeological unit (data of the aquitards not shown here). Formal statistical testing using the Mann-Whitney U-test, a nonparametric equivalent of the t-test of the equality of the mean of two samples (Davis, 2002) shows that almost all TDS across the six aquifers differ at the p = 0.05 level, except
280   between the Middle Pliocene (n_2^2) and Lower Pliocene (n_2^1) aquifers. Also, TDS in the aquifer and aquitard from the same hydrogeological unit are statistically different at the p=0.05 level. Based on this, it was decided to apply the geostatistical modeling and interpolation of TDS separately for each individual aquifer and aquitard. So, the geostatistical analysis and interpolation of TDS is performed within the volume of each individual aquifer/aquitard by using data that is located within that unit.
285   The reason for the hydrogeological units to have different statistical distributions of TDS is not clear yet. It could be due to different cycles of freshening of the erstwhile saline groundwater (Pham et al., 2019) or that mixing of saline and fresh groundwater is not uniform over the MKD. The focus of the remainder of the analysis is on the aquifers, since the main objective of the study is to assess fresh groundwater volumes. The analysis and interpolation that is reported for the aquifers is also carried
290   out for the aquitards, to obtain a 3D groundwater salinity distribution of the groundwater in the subsurface of the entire MKD, but details are not reported here.
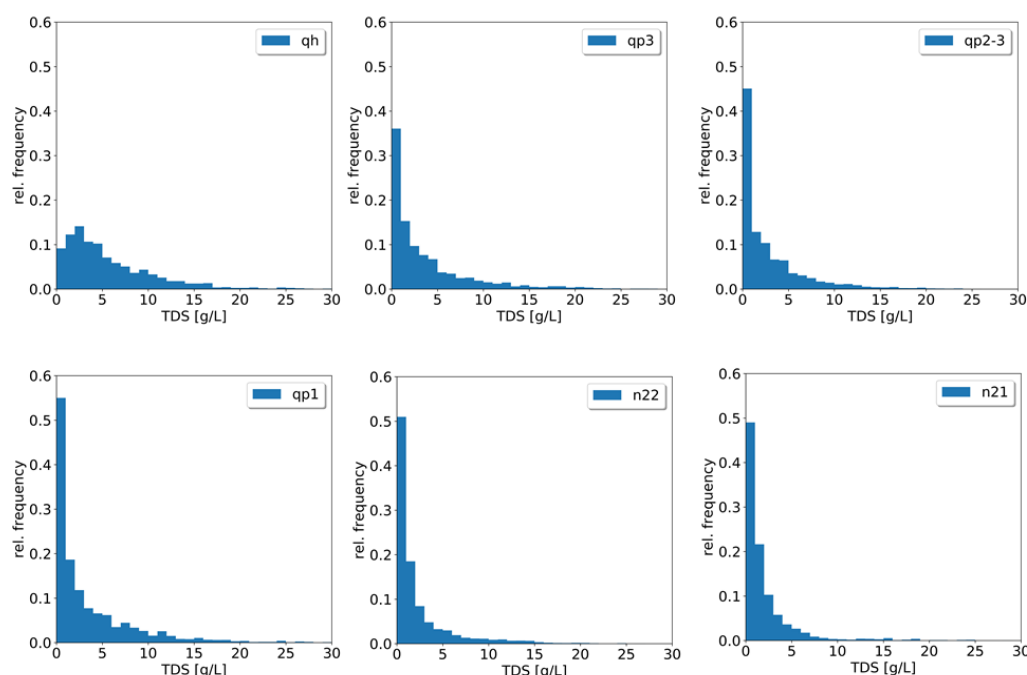
Figure 8 Statistical distributions of TDS for each aquifer.

295 The distribution of TDS is extremely skewed which makes traditional geostatistical interpolation methods such as ordinary kriging less suitable (Goovearts, 1997). One way to tackle this non-symmetry is to apply normal score transformation to obtain a Gaussian distribution (Goovaerts, 1997). Unfortunately, back-transformation into the original units is not trivial and prone to erroneous results (Deutsch and Journel, 1998). The data from the industrial extraction wells, that were uniformly set at

300 TDS of 0.3 g/L, will cause further complications due to the spike in the histogram at 0.3 g/L. Furthermore, the incorporation of "soft", incomplete data from the domestic extraction wells needs to be considered, which is difficult to achieve in a parametric setting. Indicator geostatistics allows for the incorporation of incomplete, "soft" data, by coding these into indicator values. Therefore, the indicator approach is used, in which each observation is transformed into a set of K indicator values,

305 corresponding to K threshold values. The threshold values are chosen to coincide with important TDS intervals and with more emphasis on the low TDS since that determines the quality of drinking water and usability for irrigations purposes and aquaculture. The first two threshold (0.25 g/L and 0.50 g/L) are half the recommended limit and the recommended limit for drinking water by the EPA (www.epa.gov), 1.0 g/L is the freshwater threshold in Vietnam and 3.0 g/L represents the brackish

310 water threshold. The full list of TDS indicators and their corresponding fraction at each indicator thresholds and for each hydrogeological unit is given in Table 2. The domestic wells dataset was treated as "soft data" in the data analysis, interpolation and simulation procedure. Because the domestic wells represent incomplete data – TDS concentrations are only known to be lower than 1.0 g/L – the indicator coding was performed to take this into account. So, only the indicator that

315 represents the threshold of 1.0 g/L was coded, while the rest of the indicator thresholds were assigned as missing data.

In certain areas, clusters of TDS data occur, see Fig. 4. Preferential clustering of data is detrimental to unbiased estimation and declustering is advised (Deutsch, 2002). Declustering was performed by averaging all TDS values that occur in a voxel of 1000 x 1000 x 5 m^3. This also serves to eliminate short-distance variation obscuring the regional variation. The remainder of the research described here proceeds with the declustered TDS dataset. Declustering of the data for the domestic wells was performed on a 5000 x 5000 m^2 grid spacing.

320

Table 2. Cumulative probabilities at indicator thresholds for each aquifer

unit / indicator (g/L TDS)	0.25	0.5	0.75	1	2	3	5	7.5	10	15	20	30
qh	0.03	0.06	0.08	0.10	0.22	0.36	0.56	0.72	0.82	0.93	0.96	1.00
qp3	0.18	0.23	0.31	0.36	0.52	0.61	0.76	0.84	0.90	0.95	0.98	1.00
qp2-3	0.18	0.29	0.38	0.45	0.58	0.68	0.81	0.89	0.93	0.98	0.99	1.00
qp1	0.17	0.26	0.35	0.41	0.55	0.64	0.75	0.84	0.90	0.96	0.98	1.00
n22	0.22	0.34	0.44	0.51	0.69	0.78	0.86	0.91	0.94	0.98	0.99	1.00
n21	0.18	0.32	0.40	0.49	0.71	0.81	0.90	0.95	0.97	0.98	0.99	1.00

3.2.2 Estimation of indicator semivariograms

325

The geostatistical interpolation technique (indicator kriging) calls for semivariogram models for each indicator threshold to estimate the complementary cumulative distribution function of TDS at each location (voxel). Appendix E describes the procedure for calculating the variograms and the interpretation of the results.

3.2.3 Cross-validation

330

As described in section 3.2.1, TDS data was averaged over each voxel, resulting in vertical columns of voxels (voxel-stacks) that contain TDS data that were used as input for the interpolation. To evaluate the accuracy of the interpolation, a cross-validation is carried out by discarding (for each individual aquifer) an entire stack of voxels with known TDS. Next, the ccdf of TDS for each voxel in the discarded stack is estimated. The final result of the indicator kriging cross-validation is an estimated ccdf for each 5 m interval in the cross-validated voxel stack. Since the actual TDS value is known, the performance of the interpolation can be evaluated. In this section, the results of the cross-validation for aquifer qp2-3 is given, Appendix F describes the results of the cross-validation for each aquifer. In Fig. 9 results are summarized in scatterplots and graphs.

335

340

The scatterplot (upper left panel) present the true vs. the estimated TDS (according to the E-type estimate), the correlation coefficient (r) and the mean absolute error (mae). The data contain large values of TDS that can have a great impact on the magnitude of mae. To further evaluate the results of the cross-validation, plots and bar charts are presented.

345
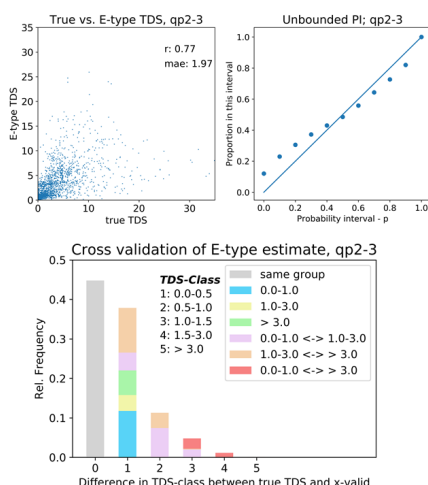
Figure 9 *Results of the cross-validation for aquifer qp2-3. Top-left shows scatterplot of True versus E-type TDS*
350   *estimate; top-right indicates the accuracy of the interpolation by proportion of data that fall in a certain*
Probability Interval (PI); lower graph shows the summary of the cross-validation results concerning grouping of
TDS values. For further explanation refer to the main text.

The accuracy plot (top, right) show the expected proportions versus the estimated proportions in 10
probability exceedance intervals (Goovaerts, 2001). In the lower probability intervals (up to probability
355   interval 0.5) the estimated proportions deviate from the theoretical proportions, indicating that the
probabilistic model for the lower probabilities is less accurate. Since the main interest is in the higher
probabilities (e.g. probability that TDS exceeds 1 g/L > 0.5), this is not regarded as problematic.

The last check concerning the performance of the interpolation was done by classifying TDS into five
classes: 0-0.5 g/L, 0.5-1 g/L, 1-1.5 g/L, 1.5-3 g/L and >3 g/L. Next, it was calculated to what extent the
360   actual and the estimated (E-type) differ ("difference in TDS-class between data and x-valid") and if so,
is the difference causing the sample to fall in another group. The grouping was done following
important TDS values for water use: 0-1 g/L (fresh), 1-3 g/L (brackish) and >3 g/L (saline). This analysis
shows that around 70% of the estimated TDS falls in the same group, although there are some
differences in classes. The number of estimated TDS that cross from fresh to saline (and vice versa) is
365   limited, and this is also the case from fresh to brackish.

Note that by allowing instrumental parameters in the interpolation to vary (e.g., neighborhood for
interpolation, minimum and maximum number of samples in the interpolation), an optimal set of
these parameters was determined such that the cross-validated results were "best" (these are the
results depicted in the graphs). No rigorous evaluation of all possible combinations of parameters was
370   performed, but the parameters were varied within reasonable limits and the results were checked
using graphs and correlation coefficients.

3.2.4 Three-dimensional modeling of TDS
3D indicator kriging is used with TDS indicator data derived from the boreholes, groundwater samples,
industrial and domestic extraction wells as input, resulting in a 3D model of the ccdf of TDS for each
375   voxel, from which the expected value of TDS (E-type estimate) was calculated. The probability that
TDS is less than a certain threshold (e.g. 1 g/L TDS) is easily computed and is also shown.

The 3D distribution of fresh-brackish-saline groundwater (classified from the E-type estimate of TDS) for the aquifers and aquitards in the MKD is depicted in Fig. 10 (left panel). The TDS were classified in 3 classes: 0-1 g/L (fresh), 1-3 g/L (brackish) and > 3g/L (saline). Together with the probability of TDS < 1g/L (right panel), this gives detailed information about the occurrence of fresh groundwater and its uncertainty.

380
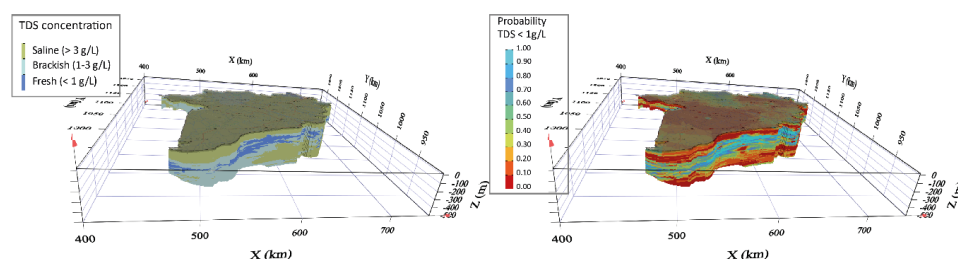
385 **Figure 10** *The 3D perspective view of the spatial distribution of fresh-brackish-saline groundwater (left panel) and the probability that TDS < 1g/L (right panel).*

The 3D model of the ccdf of TDS allows for the inspection of the fresh groundwater distribution for each individual aquifer. In Fig. 11 the models of the spatial distribution of TDS are given, again together with the probability of TDS < 1 g/L.

390
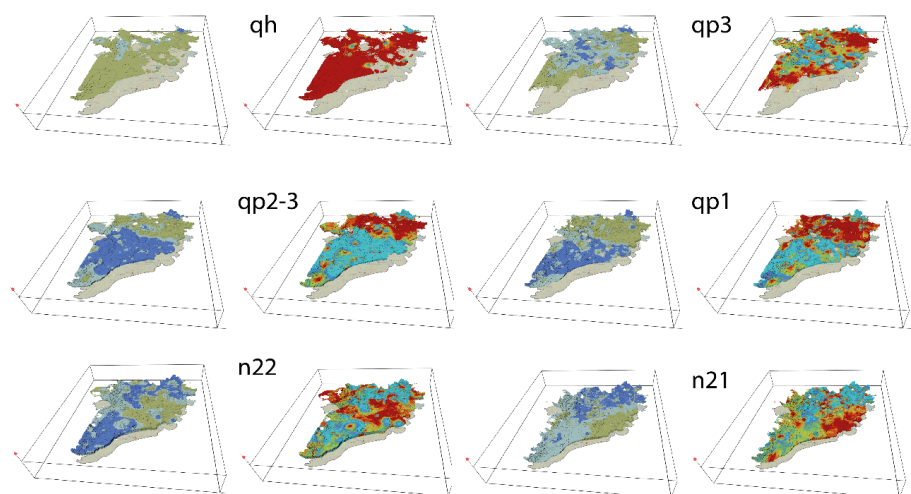
Figure 11 *3D perspective view of the spatial distribution of fresh, brackish and saline (left panels) and the probability that TDS < 1g/L (right panels) for the aquifers in the area. For legend see Figure 10*

3.2.5 Estimating the fresh groundwater volume from indicator kriging

395 For each location (*x,y*) in each aquifer the expected volume of fresh groundwater was estimated from the ccdf of TDS for each voxel in the stack and the layer-averaged drainable porosity. Assuming an upper limit for TDS of 1g/L it follows:

$$\mathrm{E}[Volume_{aquifer}(x,y)] = \left\{ \sum_{z_{bottom}}^{z_{top}} Prob\{(TDS(x,y,z)) < 1g/L\} \cdot Volume_{voxel} \right\} \cdot Drainable\ Porosity(x,y) \quad \text{(eq. 1)}$$

400 This results in the expected fresh groundwater volume at every location (Fig. 12). Adding expected volumes for each location results in the expected volume for the entire aquifer (Table 3). The total expected volume for all the aquifers considered is 867 billion m³ which is considerably larger than as a previous (most recent) estimate of 600 billion m³ (Bui et al., 2013).

Table 3. Expected volume of fresh groundwater for each aquifer (TDS < 1g/L) in billion m³

Aquifer	Volume fresh groundwater (< 1g/L TDS) in billion m³
qh	8.4
qp3	79.1
qp2-3	199.1
qp1	144.6
n22	262.3
n21	173.8

405
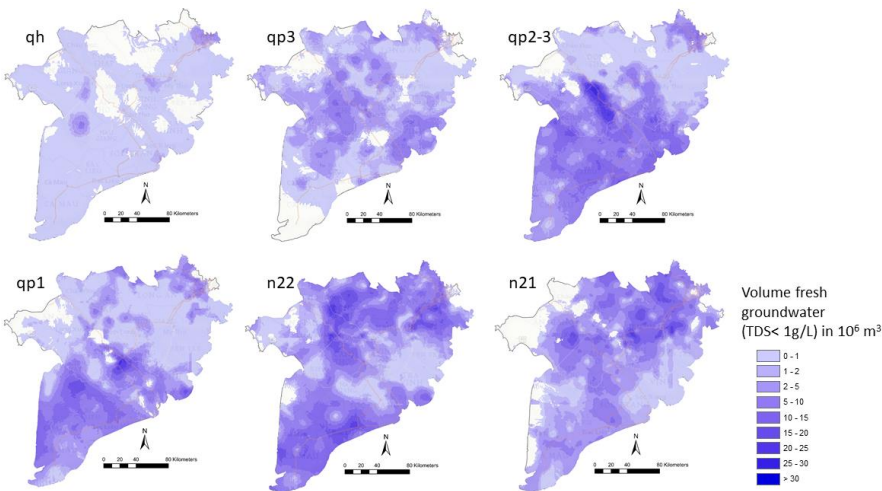
Figure 12 *Maps showing the expected depth-averaged volume of fresh groundwater in the aquifers, per 1*1km²*
model cell. In blank areas the aquifer is not present.

410

3.2.6   Uncertainty estimates of fresh groundwater volumes with indicator simulation

The fresh groundwater volume for each aquifer, as estimated with indicator kriging of TDS and drainable porosity, results in an expected value at each location, but without an indication of the uncertainty for the entire volume of the aquifer. To obtain an estimate of the uncertainty of the volumes of fresh groundwater for each aquifer, sequential indicator simulation was used to produce 100 realizations of the conditional random function of TDS for each aquifer. Again, next to the "hard" borehole and industrial extraction wells data, "soft" data from the domestic extraction wells dataset were used. The parameters that were used for indicator kriging (semivariogram model, neighborhood, etc.) were also used in simulation. For each of the 100 realizations, the volume of fresh groundwater (groundwater volume of cells with simulated TDS   < 1 g/l) was determined, resulting in 100 samples of fresh groundwater volumes for each aquifer. The resulting histograms for each aquifer are depicted in Fig. 13. As expected, the average fresh groundwater volume for each aquifer, as calculated from indicator simulation is approximately the same as resulting from indicator kriging results. The range of uncertainty is largest for the deeper aquifers, having the lowest data-density.

The uncertainty estimates of the fresh groundwater volumes calculated in this way only accounts for the spatial uncertainty of the TDS. Other sources of uncertainty, such as the uncertainty in the Formation Factor, drainable porosity and interpretation of the boreholes in hydrogeological units, are not considered.
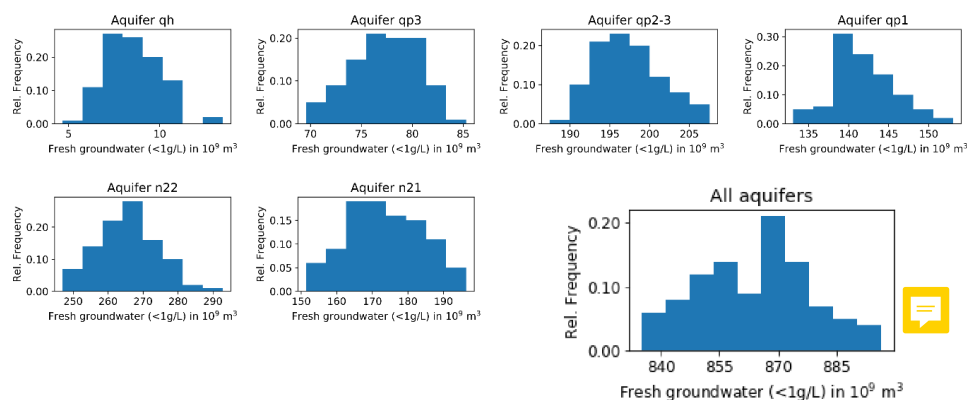
Figure 13 *Estimated volumes of fresh groundwater (TDS < 1g/L) for each aquifer and for all aquifers combined, based on 100 Monte Carlo realizations obtained by indicator simulations. Note that the units on the horizontal axes vary.*

3.2.7.   Assessing regional groundwater volumes

The estimated volume of fresh groundwater for each province was determined for each aquifer and for a range of depth intervals, (rel. to MSL): < -50 m, -50 m - -100 m, -100 m - -200 m and < -200 m. In Fig. 14 the results are presented, together with the uncertainty, based on indicator simulation. There is considerable variation in the availability of fresh groundwater over the provinces and depth ranges.
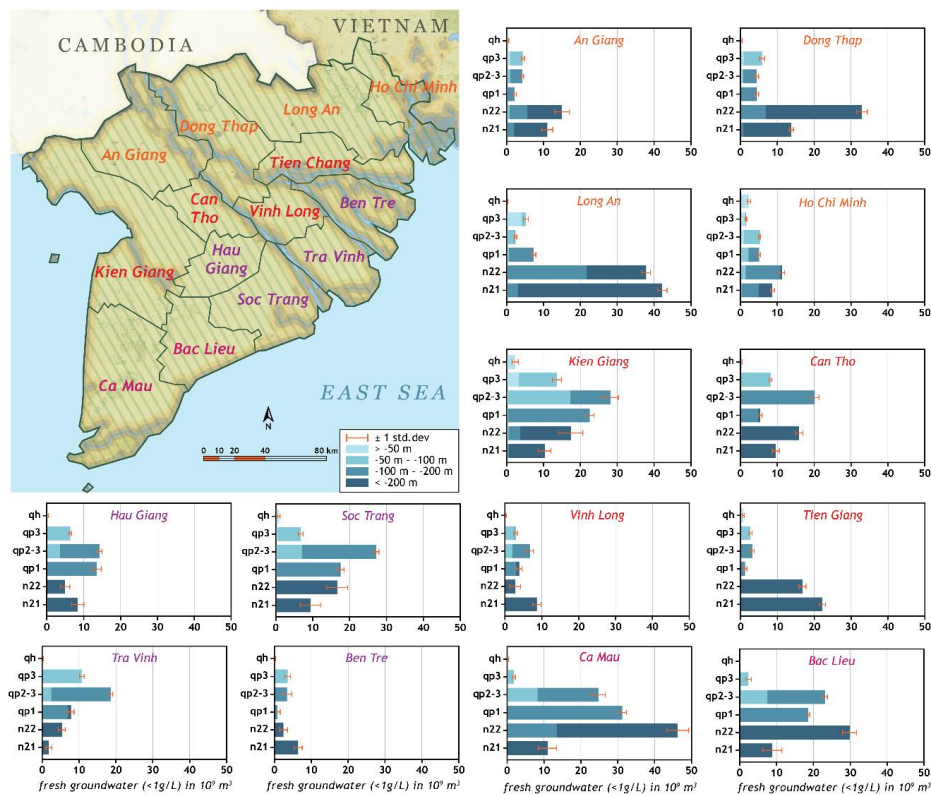
Figure 14 *Volume of fresh groundwater in the aquifers for each province and depth interval (rel. to MSL), including uncertainty. Copyright map, see Fig. 1.*

4. Conclusions

For the Mekong delta, Vietnam, data from various sources (boreholes with geophysical loggings, groundwater samples, industrial extraction wells and "soft" domestic wells) data were combined to produce a 3D model of the ccdf of TDS, representing the groundwater salinity distribution. The first step was to construct a 3D hydrogeological model so that the groundwater salinity modeling could proceed within the constraints of the fresh groundwater volume of each aquifer and aquitard. By using the geostatistical interpolation technique indicator kriging, it was possible to combine TDS data from different sources and quality to produce a ccdf of TDS at each (x,y,z) location. The results of the interpolation and simulation indicate that there is a sizable fresh groundwater volume in the MKD area (an expected value of 867 billion m³, with an uncertainty range of 830-900 billion m³). There is considerable spatial variability in TDS, and the uncertainty in volumes is the largest for the deeper aquifers. With this groundwater salinity model containing both TDS concentrations and uncertainties, a tool for the management of fresh groundwater reserves is available that can help to promote and manage sustainable use of this precious freshwater source.

The fresh groundwater volume seems to be huge, in comparison with the present yearly groundwater extraction rates for industrial, domestic and agricultural water use. However, it is important to recognize that in areas where replenishment is limited these extraction rates can cause rapid upconing of brackish to saline groundwater. Mixing of fresh groundwater with brackish and/or saline groundwater is a serious threat to the fresh groundwater volume and makes that an apparently modest groundwater extraction regime can easily become non-sustainable.

Acknowledgements

The Division of Water Resources Planning and Investigation for the South of Vietnam, Ho Chi Minh city, Vietnam is thanked for providing subsurface and hydrological data for this research. This paper is part of PhD research carried out by Hung Van Pham at the Department of Physical Geography, Utrecht University, The Netherlands. The PhD project is funded by NWO-WOTRO (W 07.69.105), Deltares and TNO-Geological Survey of the Netherlands. The work described in this publication was supported by NWO-WOTRO's Urbanizing Deltas in the World program through the grant to the budget of the Rise and Fall project, Grant: W07.69.105.

Data availability

The hydrogeological model and the model of TDS (E-type estimate and probability TDS < 1g/L) can be accessed from https://doi.org/10.5281/zenodo.4441776 (Gunnink et al, 2021).

Appendix A

Hydrogeological schematization in the MKD

A highly heterogeneous stratigraphy was formed in the MKD as a result of repeated transgression and regression events from the late Neogene to the present. The Pleistocene and Holocene sediments are of fluvial and a deltaic origin, while Miocene and Pliocene sediments are of marine origin (Bui et al., 2013). The sediments in the MKD can be divided into seven geological units (Minderhoud et al, 2017; Pham et al., 2019). Each geological unit consists (in general) of a lower part of fine to coarse sand (aquifer) and an upper part of silt, sandy clay and clay (aquitard). The hydrogeological schematization of aquifers and aquitards in the MKD is depicted in Fig. A1. According to the Vietnamese nomenclature (Bui et al., 2013; Nguyen et al., 2004), the seven aquifers (lower case) / aquitards (upper case) in the study area are: Holocene (qh / Q_2), Late Pleistocene (qp_3 / Q_1^3), Late - middle Pleistocene (qp_{2-3} / Q_1^{2-3}), Early Pleistocene (qp_1 / Q_1^1), Middle Pliocene (n_2^2 / N_2^2), Early Pliocene (n_2^1 / N_2^1) and Late Miocene (n_1^3 / N_1^3). The MKD unconsolidated sediments are very thick, especially near the coast where between the two main rivers thicknesses up to nearly 600 m are observed (Nguyen et al., 2004). For reference, only 0.3% of the coastal aquifers in the world are estimated to exceed this thickness (Zamrsky et al., 2018).
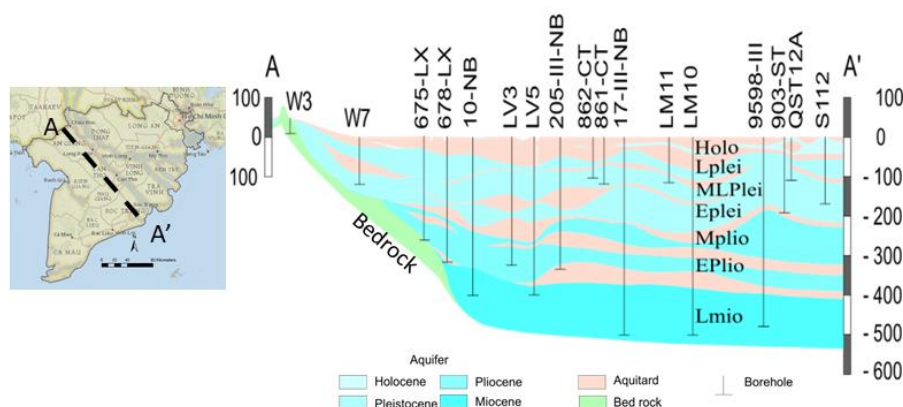
Figure A1 *The setting and hydrogeological features of the Mekong Delta, Vietnam with the locations of the cross-sections AA' (from Doan et al., 2016). Copyright map, see Fig. 1.*

495 ***Appendix B***

Formation Factor

The intrinsic Formation Factor (Archie, 1942) - F_i - is only valid for clay-free, clean, consolidated sediments. For unconsolidated, clayey sediments, the apparent Formation Factor - F_a - is defined as the ratio of bulk resistivity over fluid resistivity. A modification of the Archie equation is proposed by

500 Huntley (1986) and Worthington (1993) and applied by e.g. Soupios et al. (2007) and Faneca Sànchez et al. (2012), to obtain F_a.

The relation between F_i and F_a is given by:

$1/F_a = 1/ F_i + (BQ_v/ F_i) * \rho_w$ (Eq. B1)

where BQ_v is related to the effects of surface conduction, mainly due to clay particles and ρ_w is the

505 resistivity of the groundwater. When plotting $1/ F_a$ vs. ρ_w, the intercept of the straight line with the y-axis will result in $1/ F_i$ and BQ_v / F_i represents the gradient. Since there are no data of F_i available for the sediments in the Mekong Delta, published data from De Louw et al. (2011) and Faneca Sànchez et al. (2012) was used. These F_i were determined in unconsolidated Holocene and Pleistocene sediments in the Rhine-Meuse delta Netherlands, which is thought to be applicable to the Mekong Delta

510 sediments, due to the similarity in depositional environments and lithology in both deltas.

The F_i values were checked for validity in the following way. The dataset from DWIPRS contains lithology, TDS and LN64 (bulk resistivity) for 55 depth intervals, covering the main hydrogeological units and lithologies therein in the MKD, but the dataset contains no data on groundwater resistivity, ρ_w.

515 Buschmann et al. (2008) reported data on TDS and ρ_w in the Mekong Delta of Vietnam, for 112 samples with an average sampling depth of 70 m (range 10 m – 420 m). An et al. (2014) collected 22 samples of TDS and ρ_w in a coastal area in the eastern part of the Mekong Delta from depths 80 – 130 m. These two datasets were merged and a linear regression between TDS and electrical conductivity (Ec) of the

Open Access   Earth System
Science Data
Discussions

groundwater (the reciprocal of ρ_w and corrected for temperature, according to TNO-IGG, 1992) is
520 established, Fig. B1. This regression is applied to the measured TDS in the DWIRPS database to derive
(again, after correction for temperature) ρ_w. This allows for the calculation of the apparent Formation
Factor, F_a.
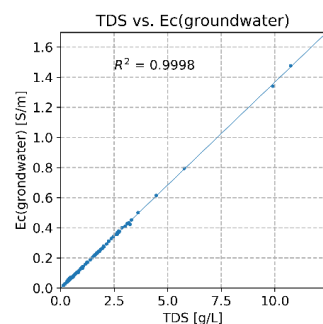
525 **Figure B1** *Linear relation between TDS and Ec(groundwater), based on data from Buschmann et al. (2008) and An et al. (2014).*

The Formation Factor depends on the lithology of the sediments, especially the clay content. The
applicability of the published F_i in this study was checked for each lithology class by applying the
relation of Fig. B1 to the measured TDS to obtain ρ_w and subsequently obtaining $1/F_a$ is for the
530 lithological units of Table 1, see Fig. B2.

There is scatter in most of the graphs, caused by variability in grain size of the sand fraction, clay
content and facies change. In general, F_i derived from the analysis depicted in Fig. B2 confirms the
applicability of initial F_i from de Louw et al. (2011) and Faneca Sànchez et al. (2012) that were used in
this study.

535
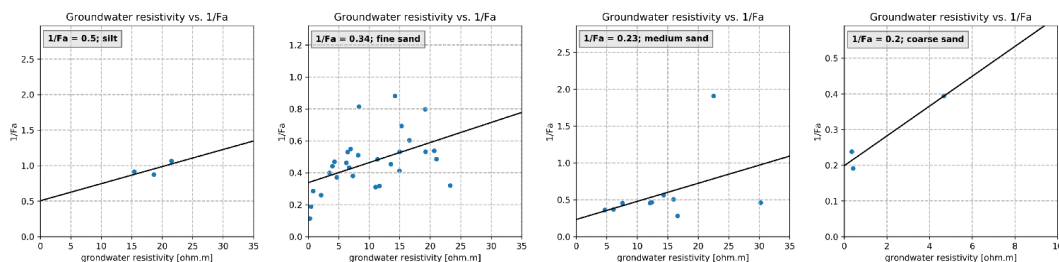
Figure B2 *Relation between groundwater resistivity and $1/F_a$ for four lithologies, from which F_i can be obtained.*

Appendix C

540   *Drainable porosity*

Average drainable porosity for aquifers in MKD is presented in Shrestha et al. (2016), based on max. 9 measurements per aquifer. It turned out that the data on drainable porosity is based on an un-published mathematical transformation using horizontal hydraulic conductivity measurements, which are derived from pumping tests. The drainable porosity values (viz. 0.12 - 0.18) seem to be

545   small with respect to the coarseness of the sediment, as described in the boreholes. Pechstein et al. (2018) present results of a pumping test in the Ca Mau province, with an average drainable porosity for the n_2^2 aquifer of 0.22. Although this is only a single measurement, the drainable porosity seems to be more in line with what would be expected, given the coarseness of the sediments. To derive a spatially variable drainable porosity, borehole intervals were assigned drainable porosity values that

550   depend on lithology. Values for lithology-dependent drainable porosity were derived from literature, especially Johnson (1967) which contains an in-depth analysis of drainable porosity for aquifers in the United States, based on the analysis of pumping tests in which the lithology of the aquifer was also described. The lithological description from Johnson (1967, table 29) is therefore linked to the lithology of the boreholes in the MKD, and the corresponding drainable porosity assigned, see Table

555   1. To obtain a value of drainable porosity for each aquifer at borehole locations that is representative for the entire depth-interval covering the aquifer, the weighted average of the drainable porosities of all the depth-intervals that belong to the aquifer was calculated. Finally, depth-averaged drainable porosity maps per aquifer were obtained by interpolating between boreholes using ordinary kriging.

560   The results of the interpolation are depicted in Fig. C1. It turned out that the kriging variance (as a measure of the interpolation uncertainty) is small, with a Coefficient of Variation (CV) < 10%. Therefore, the effect of interpolation uncertainty of the drainable porosity in the calculation of fresh groundwater volumes is discarded.
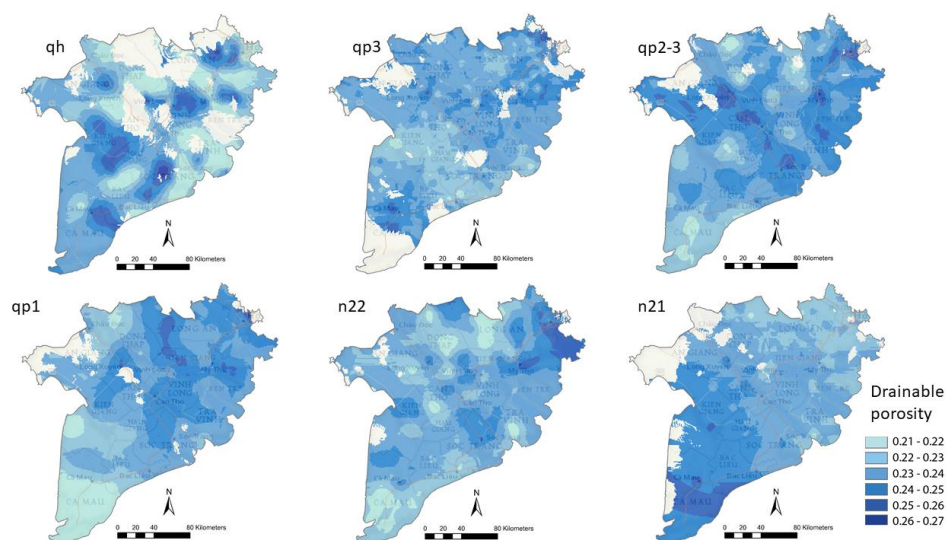
565   *Figure C1 Maps of layer-average drainable porosity for aquifers in the MKD as obtained from ordinary kriging. In blank areas the aquifer is not present*

Appendix D

570   *Hydrogeological model*

For each unit, boreholes were selected that penetrate through that entire unit and the base of the hydrogeological unit was determined. This new base was then compared to the base of the old, basic model of Minderhoud (2017) at that location and the residual (difference between the basic model and the base of the unit from the interpreted borehole) was interpolated using ordinary

575   kriging. After adding the interpolated residual to the old basic model of Minderhoud (2017), an updated and more detailed model of the base of each hydrogeological unit was obtained. The next step was to compare this updated model with the boreholes that did not penetrate the entire unit and, if necessary, to adjust the model. If the borehole that did not penetrate the entire hydrogeological unit encountered the new base of the updated model, the base of that unit in the

580   borehole was assumed to be equal to the its current base, plus an additional 5 m (the thickness of the voxel in the 3D model). The interpolation procedure was then repeated until the base of all non-penetrating boreholes comply with the interpolated base. Results are depicted in Fig. D1.
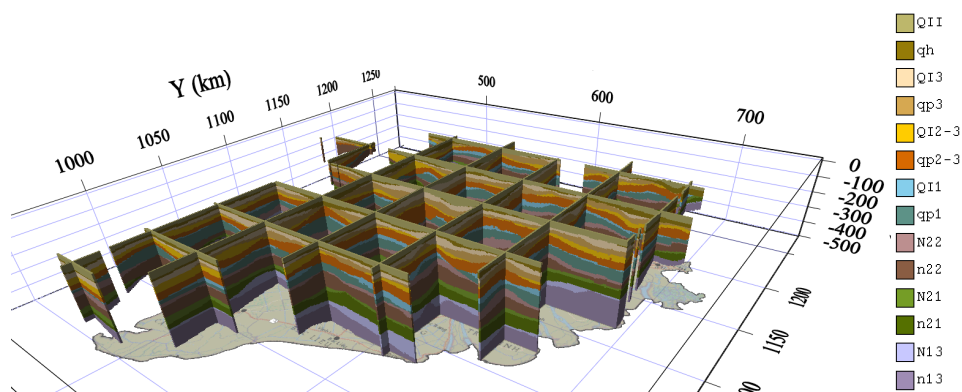
585   ***Figure D1*** *Cross-sections through the updated hydrogeological model. Scale according to kilometer reading along the axis (km) and depth in meters. Vertical exaggeration 100x; aquifers (lower case names) and aquitards (upper case names).*

Appendix E

590   *Variogram analysis of TDS*

To alleviate the burden of variogram inference (14 units, 11 indicators), the median indicator kriging approach was adopted, in which the semivariogram for the median of the distribution (TDS of 1 g/L for all units) was used for all indicators. Research showed that there are only minor differences in interpolation results between full indicator kriging and median indicator kriging (Goovaerts, 2009).

595   Experimental semivariograms and the semivariogram models for the median indicators are depicted in Fig. E1 for the six aquifers. From the experimental semivariograms it becomes clear that anisotropy

in the horizontal plane is not apparent from the data: the experimental semivariograms for the Northwest – Southeast (N310) direction – the direction of flow of the fluvial system - are not fundamentally different from those in the direction perpendicular (N40). This indicates that the
600   salinization of the (presumed) formerly fresh aquifers did occur independent from the (current) river flow direction. This confirms with the concept of salinization of the groundwater as a consequence of widespread transgression during 12 ka – 2.5 ka before present (Pham et al., 2019). The vertical semivariograms show a spatial correlation distances up to tens of meters, indicating a strong continuity in TDS values in the vertical direction. The horizontal ranges of the semivariogram models
605   are comparable to those found by Hoang (2008) for Pleistocene aquifers in Vietnam (Red River Delta), that also showed almost no horizontal anisotropy.
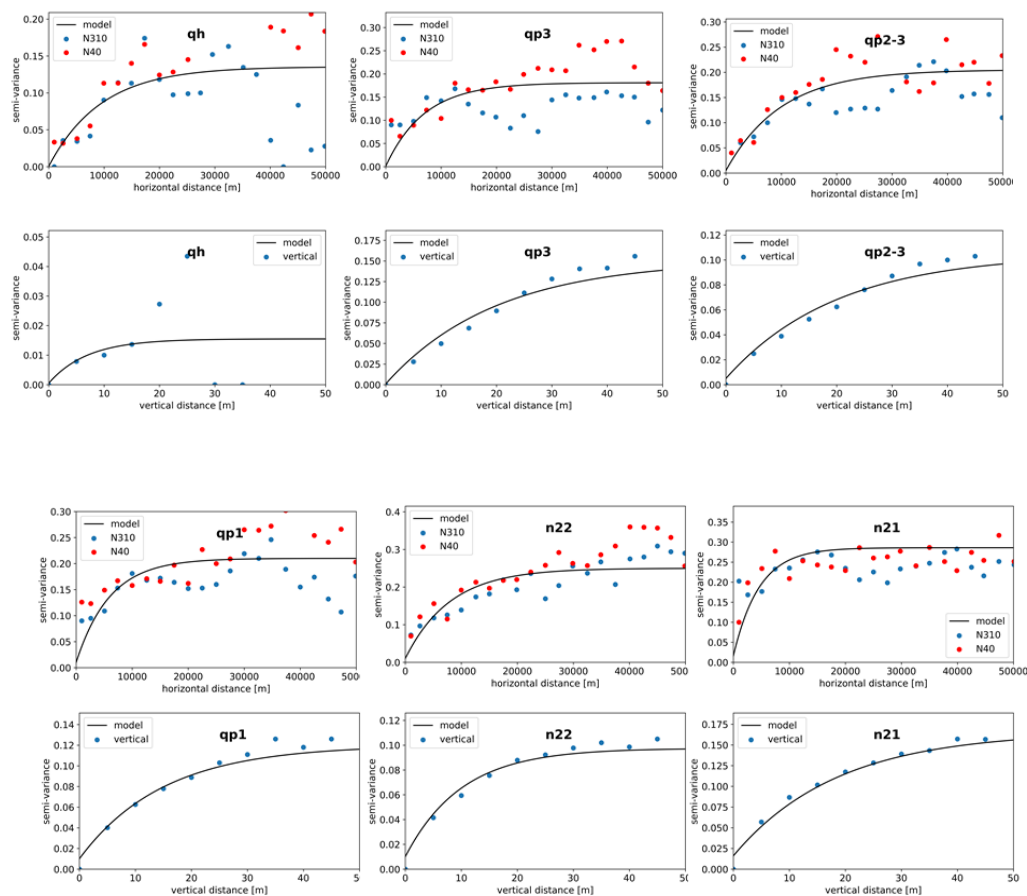
610   ***Figure E1** Horizontal and vertical experimental Indicator semivariograms at indicator TDS=1.0 g/L and fitted exponential semivariogram models.*

Appendix F

Cross-validation of TDS

615

The cross-validation results for all aquifers are presented in Fig. F1. For a description of the graphs
see section 3.2.3 in the main text.
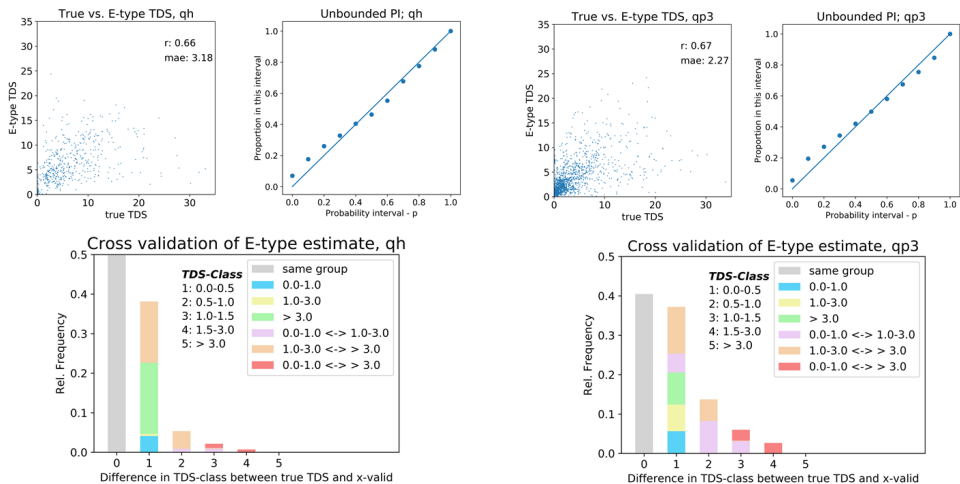
620
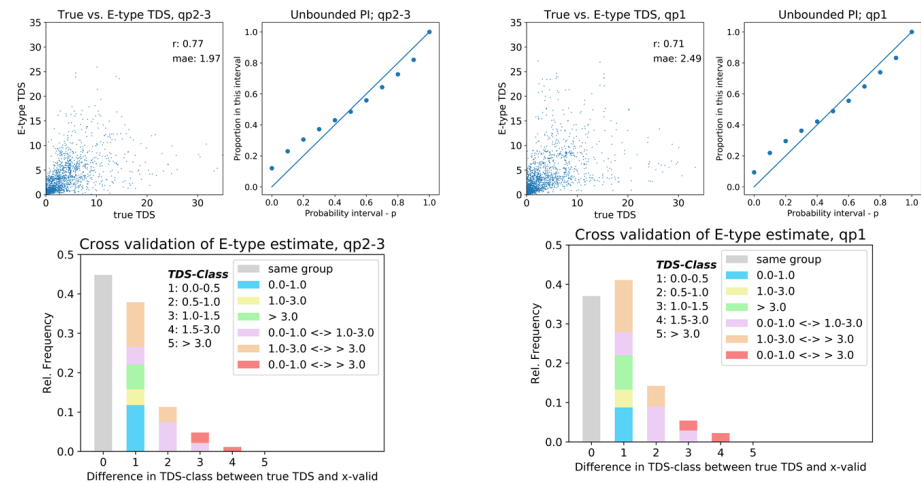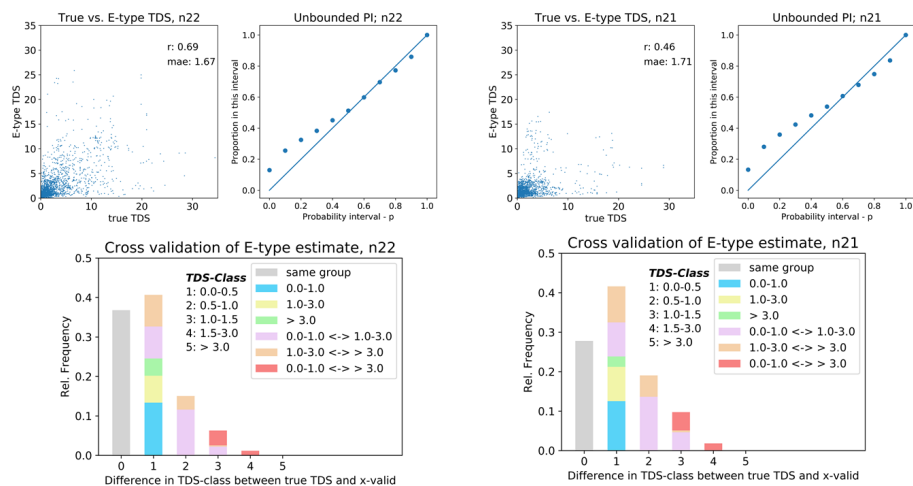
Figure F1 *Results of the cross-validation per aquifer. Top-left shows scatterplot of True versus E-type TDS*
estimate; top-right indicates the accuracy of the interpolation by proportion of data that fall in a certain
Probability Interval (PI); lower graph shows the summary of the cross-validation results concerning grouping of
TDS values. For further explanation refer to the main text.

Author contribution

HVP collected and prepared the data and performed the first data analysis. JG and HVP designed the
research set-up and JG carried out the analysis. GOE and MB contributed to the interpretation. JG
prepared the manuscript with contributions from all co-authors.

Competing interests

The authors declare that they have no conflict of interests.

References

An, T. D., Tsujimura, M., Le Phu, V., Kawachi, A., & Ha, D. T.: Chemical characteristics of surface water
and groundwater in Coastal Watershed, Mekong Delta, Vietnam. Procedia Environmental
Sciences, 20, 712–721, 2014.

Archie, G.E.: The electrical resistivity log as an aid in determining some reservoir characteristics,
Petroleum Transactions of AIME, 146, pp. 54-62, https://doi.org/10.2118/942054-G,
1942.

Bui, T.V., Ngo, D.C., Le, H.N., Dang, V.T.: Assessment of Climate Change on Groundwater Resources in
Mekong Delta, Proposal of Adaptation Measures, Division of Water Resources and Planning
Investigation for the South of Viet Nam, Ho Chi Minh City, Vietnam, 2013.

Buschmann, J., Berg, M., Stengel, C., Winkel, L., Sampson, M.L., Pham Thi Kim Trang, P.T.K., Viet,
P.H.: Contamination of drinking water resources in the Mekong delta floodplains:
Arsenic and other trace metals pose serious health risks to population, Environment International 34

(2008) 756–764, https://doi.org/10.1016/j.envint.2007.12.025, 2008.

Caers, J., 2011. Modeling uncertainty in the Earth Sciences. Wiley-Blackwell, West-Sussex, UK, pp. 229.

655   Coleman J.M. and Roberts H.H.: Deltaic coastal wetlands. In: Van der Linden, W.J.M., Cloetingh, S.A.P.L., Kaasschieter, J.P.K., Van de Graaff, W.J.E., Vandenberghe, J., Van der Gun, J.A.M. (Eds). Coastal Lowlands, Springer, Dordrecht, The Netherlands. pp 1–24, https://doi.org/10.1007/978-94-017-1064-0_1, 1989.

660   Davis, J.C.: Statistics and data analysis in Geology. Wiley , New Jersey, pp. 656, 2002.

De Louw, P.G.B., Eeman, S., Siemon, B., Voortman, B.R., Gunnink, J.L., Van Baaren, E.S., Oude Essink, G.H.P.: Shallow rainwater lenses in deltaic aras with saline seepage, Hydro. Earth Syst. Sci., 15, 3659-3678, https://doi.org/10.5194/hess-15-3659-2011, 2011.

665

Deutsch, C.V and Journel, A.G.: GSLIB: Geostatistical Software Library and User's guide, 2nd edn. Oxford University Press, New York, pp. 369, 1998.

Deutsch, C.V.: Geostatistical Reservoir Modeling. Oxford University press, New York, pp. 376, 2002.

670

Doan, N.T., Bui, T.V., Bui, S.C.: Remapping the Hydrogeological Map in Southern Part of Vietnam, Scale 1:200.000, Division of Water Resources and Planning Investigation for the South of Viet Nam, Ho Chi Minh City, Vietnam, 2016.

675   Erban, L.E., Gorelick, S.M. and Zebker, H.A., Fendorf, S.: Release of arsenic to deep groundwater in the Mekong Delta, Vietnam, linked to pumping-induced land subsidence, PNAS, August 20, 2013, vol. 110, no. 34, pp 13751-13756, https://doi.org/10.1073/pnas.1300503110, 2014.

Erban, L.E., Gorelick, S.M. and Zebker, H.A.: Groundwater extraction, land subsidence, and sea-level
680   rise in the Mekong Delta, Vietnam, Environ. Res. Lett., 9(8), https://doi.org/10.1088/1748-9326/9/8/084010, 2014.

Faneca Sànchez , F., Gunnink, J.L., Van Baaren, E.S., Oude Essink, G.H.P., Siemon, B., Auken, E., Elderhorst, W., De Louw, P.G.B.: Modeling climate change effects on a Dutch coastal groundwater
685   system using airborne electromagnetic measurements, Hydrol. Earth Syst. Sci., 16, 4499-4516, https://doi.org/10.5194/hess-16-4499-2012, 2012.

Faneca Sànchez, M., Bashar, K., Janssen, G.M.C.M., Vogels, M., Snel, J., Zhou, Y., Stuurman, R.J., Oude Essink, G.H.P.: SWIBANGLA: Managing salt water intrusion impacts in coastal groundwater systems of
690   Bangladesh, https://doi.org/10.13140/2.1.1793.1042, 2015.

Fitts, C.R.: Groundwater Science. Academic Press, London, UK, pp. 450, 2002.

Giosan, L.L., Syvitski, J.P.M., Constantinescu, S., Day, J.W.: Protect the worlds delta's, Nature 516, 31-
695   33. https://doi.org/10.1038/516031a, 2014.

Goovaerts, P: Geostatistics for Natural Resources Evaluation, Oxford University Press, New York, pp.
512, 1997.

700   Goovaerts, P.: Geostatistical modeling of uncertainty in soil science. Geoderma 103 (2001) 3-
26, https://doi.org/10.1016/S0016-7061(01)00067-2, 2001.

Goovaerts, P.: AUTO-IK: A 2D indicator program for the automated non-parametric modeling of local
uncertainty in earth sciences, Computer & Geosciences, 35, 1255-1270, https://doi.org/
705   10.1016/j.cageo.2008.08.014, 2009.

Gunnink, J.L., Van Pham, H., Oude Essink, G.H.P, Bierkens, M.F.P.: 3D Hydrogeological and TDS model
of the Mekong delta, Vietnam; link to NetCDF file at https://doi.org/10.5281/zenodo.4441776, 2021.

710   Hamer, T., Dieperink, C., Van Pham Dang Tri, Otter, H.S., Hoekstra, P.: The rationality of groundwater
governance in the Vietnamese Mekong Delta's coastal zone, International Journal of Water Resources
Development, 36 (1), 127-148, https://doi.org/10.1080/07900627.2019.1618247, 2019.

Hoang, D.N.: Geostatistical tools for better characterization of the groundwater quality – case studies
715   for the coastal Quaternary aquifers in the Nam Dinh area, Vietnam, PhD thesis, Greifswald, Germany,
2008.

Huntley, D.: Relations between permeability and electrical resistivity in granular aquifers,
Groundwater 24 (4), 466– 474, https://doi.org/10.1111/j.1745-6584.1986.tb01025.x, 1986.

720

Jenn, F., Hoàng Thị Hạnh, Lê Hoài Nam, Pechstein, A., Nguyễn Thị Anh Thư: Baseline Study Cà Mau;
Review of studies on groundwater resources in Ca Mau Province, IGPVN Technical Report III-2,
Hannover, Germany, 2017.

725   Johnson, A.I.: Drainable porosity – compilation of drainable porosities for various materials. Geological
Survey water-supply paper 1662-D, 1967.

Journel, A. G.: Nonparametric-estimation of spatial distributions, Mathematical Geology 15, 445-468,
https://doi.org/10.1007/BF01031292, 1983.

730

Journel, A.G. and Huijbregts, CH. J.: Mining Geostatistics. Academic Press, London, 1978.

Larsen, F., Tran, L.V., Hoang, H. Van, Tran, T.L., Christiansen, A.V., Pham, N.Q.: Groundwater salinity influenced by Holocene seawater trapped in incised valleys in the Red River delta plain, Nat. Geosci. 10, 376–381, https://doi.org/10.1038/ngeo2938, 2017.

Li, J. and Heap, A.D.: A Review of Spatial Interpolation Methods for Environmental Scientists, Geoscience Australia, Record 2008/23, 137 pp, 2008.

Minderhoud, P.S.J., Erkens, G., Van Hung, P., Vuong, B.T., Erban, L.E., Kooi, H. and Stouthamer, E.: Impacts of 25 years of groundwater extraction on subsidence in the Mekong delta, Vietnam, Environ. Res. Lett., 12, 13, https://doi.org/10.1088/1748-9326/aa7146, 2017.

Minderhoud, P.S.J., Coumou, L., Erkens, G., Middelkoop, H., Stouthamer, E.: Mekong delta much lower than previously assumed in sea-level rise impact assessments, Nat. Commun. 10, 1–13, https://doi.org/10.1038/s41467-019-11602-1, 2019.

Nguyen, H. T. and Gupta, A. D.: Assessment of water resources and salinity intrusion in the Mekong Delta, Water Int., 26(1), 86–95, https://doi.org/10.1080/02508060108686889, 2001.

Nguyen, H.D., Tran, V.K., Trinh, N.T., Pham, H.L., Le, D.N.: Research of geological structure and classification of N-Q sediments in Vietnamese Mekong Delta. Division of Geology and Minerals of the South of Viet Nam, Ho Chi Minh City, Viet Nam, 2004.

Pechstein, A., Hanh, H.T., Orilski, J., Nam, L.H., Manh, L.V.: Detailed investigation on the hydrological situation in Ca Mau Province, Mekong Delta, Vietnam, Technical report III-5, Project: Improvement of Groundwater Protection in Vietnam (IGPVN), 2018.

Pham, H.V., Van Geer, F.C. , Tran, V.B., Dubelaar, W., Oude Essink, G.H.P.: Paleo-hydrogeological reconstruction of the fresh-saline groundwater distribution in the Vietnamese Mekong Delta since the late Pleistocene, J. Hydrol. Reg. Stud., 23, 100594, https://doi.org/10.1016/j.ejrh.2019.100594, 2019.

Rahman, M.M., Penny, G., Mondal, M.S., Zaman, M.H., Kryston, A., Salehin, M., Nahar, Q., Islam, M.S., Bolster, D., Tank, J.L., Müller, M.F.: Salinization in large river deltas: Drivers, impacts and socio-hydrological feedbacks, Water Secur. 6, 100024, https://doi.org/10.1016/j.wasec.2019.100024, 2019.

Renaud, F.G. and Kuenzer, C.: The Mekong Delta System; Interdisciplinary Analyses of a River Delta, Springer Environmental Science and Engineering, pp. 466. https://doi.org/10.1007/978-94-007-3962-8, 2012.

Saisna, M., G. Dubois, A. Chaloulakou, N. Spyrellis,: Classification criteria and probability risks maps:

limitations and perspectives, Environ. Sci. Technol, 38, 5, 1275-1281, https://doi.org/10.1021/es034652+, 2004.

775   Shrestha, S., Bach, T. V., Pandey, V. P.: Climate change impacts on groundwater resources in Mekong Delta under representative concentration pathways (RCPs) scenarios, Environ. Sci. Policy, 61, 1–13, https://doi.org/0.1016/j.envsci.2016.03.010, 2016.

Soupios, P.M., Kouli, M., Vallianatos, F., Vafidis, A., Stavroulakis, G.: Estimation of aquifer hydraulic
780   parameters from sirficial geophysical methods: A case study of Keritis Basin in Chania (Crete – Greece), Journal of Hydrology (2007) 338, 122-131, https://doi.org/10.1016/j.jhydrol.2007.02.028, 2007.

Syvitski, J.P.M., Kettner, A.J., Overeem, I., Hutton, E.W.H., Hannon, M.T., Brakenridge, G.R., Day, J.W., Vörösmarty, C.J., Saito, Y., Giosan, L., Nicholls, R.J.: Sinking deltas due to human activities, Nat. Geosci.
785   2, 681–686, https://doi.org/10.1038/ngeo629, 2009.

Tam, V. T., Batelaan, O., Le, T. T. and Nhan, P. Q.: Three-dimensional hydrostratigraphical modeling to support evaluation of recharge and saltwater intrusion in a coastal groundwater system in Vietnam, Hydrogeol. J., 22(8), 1749–1762, https://doi.org/10.1007/s10040-014-1185-2, 2014.
790

Tessler, Z.D., Vörösmarty, C.J., Grossberg, M., Gladkova, I., Aizenman, H., Syvitski, J.P.M., Foufoula-Georgiou, E.: Profiling risk and sustainability in coastal deltas of the world, Science, vol. 349, Issue 6248, pp. 638–643, https://doi.org/10.1126/science.aab3574, 2015.

795   TNO-IGG: Introduction to geophysical well logs, a practical course for groundwater studies. TNO Instituut voor Grondwater en Geo-Energie, Delft (in Dutch), 1992.

Tran, L.T., Larsen, F., Pham, N.Q., Christiansen, A.V., Tran, N., Vu, H.V., Tran, L.V., Hoang, H.V. and Hinsby, K.: Origin and extent of fresh groundwater, salty paleowaters and recent saltwater intrusions
800   in Red River flood plain aquifers, Vietnam, Hydrogeol. J., 20(7), 1295–1313, https://doi.org/10.1007/s10040-012-0874-y, 2012.

Van Engelen, J., Verkaik, J., King, J., Nofal, E.R., Bierkens, M.F.P. and Oude Essink, G.H.P.: A three-dimensional paleo-reconstruction of the groundwater salinity distribution in the Nile Delta Aquifer.
805   Hydrol, Earth Syst. Sci. 23, 5175–5198, https://doi.org/10.5194/hess-2019-151, 2019.

Van, T. P. and Koontanakulvong, S.: Estimation of Groundwater Use Pattern and Distribution in the Coastal Mekong Delta, Vietnam via Socio-Economical Survey and Groundwater Modelling, Engineering Journal, 23 (6), 487-499, https://doi.org/10.4186/ej.2019.23.6.487, 2019
810

Wada, Y., Van Beek, L.P.H., Viviroli, D., Dürr, H.H., Weingartner, R. and Bierkens, M.F.P.: Global monthly water stress: 2. Water demand and severity of water stress, Water Resour. Res. 47, 1–17. https://doi.org/10.1029/2010WR009792, 2011.

815   Wagner, F., Tran, V.B., Renaud, F.G.: Chapter 7, groundwater resources in the Mekong Delta: availability, utilization and risks. In: Kuenzer, C., Renaud, F. (Eds.), The Mekong Delta System, 201–220, https://doi.org/10.1007/978-94-007-3962-8-7, 2012.

        Worthington, P.F.: The uses and abuses of the Archie equations: 1. The formation factor–porosity
820   relationship, Journal of Applied Geophysics 30, 215–228, https://doi.org/10.1016/0926-9851(93)90028-W, 1993.

        www.epa.gov; website accessed December 2019.

825   Zamrsky, D., Oude Essink, G.H.P., Bierkens, M.F.P.: Estimating the thickness of unconsolidated coastal aquifers along the global coastline. Earth System Science Data, 10, 1591-1603, https://doi.org/10.5194/essd-10-1591-2018, 2018

830